Geomechanics for Energy and the Environment 47 (2026) 100855

Contents lists available at ScienceDirect

Geomechanics for Energy and the Environment

journal homepage: www.elsevier.com/locate/gete

Assessment of measurement techniques to monitor engineered barrier systems for nuclear waste repository

Bruna de Carvalho Faria Lima Lopes [a], Alessandro Tarantino [b,*]

[a] Department of Civil and Environmental Engineering, Pontifícia Universidade Católica do Rio de Janeiro (PUC-Rio), Rio de Janeiro, Brazil
[b] Department of Civil and Environmental Engineering, University of Strathclyde, Glasgow, UK

ARTICLE INFO

Editor-in-Chief: Dr A Ferrari

Keywords:
Bentonite
Electrical conductivity
Relative dielectric permittivity
Suction
Water retention
Engineered barrier
Nuclear waste repository

ABSTRACT

A major challenge in the implementation of Engineered Barrier Systems (EBS) for the geological disposal of nuclear waste is monitoring their response to thermal and hydraulic loading. This applies to mock-up scale tests designed to validate the EBS concept via 'wired' local sensors, but also to future full-scale EBSs to be monitored 'wireless' via electrical geophysical techniques for EBS validation during the operational stage. To underpin the monitoring of EBS, this study investigates experimental techniques for measuring the volumetric water content, suction, and electrical conductivity of bentonite-based materials. It is demonstrated that Time Domain Reflectometry (TDR) probes can be successfully used to monitor volumetric water content provided that i) the measured apparent relative dielectric permittivity is corrected for the effect of clay electrical conductivity and ii) the calibration equation accounts for the effect of bulk density and adsorbed water. It was also shown that the electrical conductivity inferred from TDR and direct current four-point method measurements may differ substantially, and such a difference can be associated with the frequency-dependent contribution of free and adsorbed water to bulk electrical conductivity. Finally, encapsulated Micro-Electro-Mechanical Systems (MEMS) sensors were demonstrated to measure total suction with satisfactory accuracy over the full relative humidity range.

1. Introduction

The geological disposal of nuclear waste relies on a combination of natural and engineered barriers to ensure long-term isolation of radioactive materials from the biosphere.[1–5] Within this framework, Engineered Barrier Systems (EBS) play a central role by providing a controlled physical and chemical environment that limits radionuclide migration and ensures repository safety over geological timescales.[1–3,5–9] The performance of EBS must therefore be demonstrated not only at the design stage, but also throughout their operational and post-closure evolution.[10]

Monitoring the response of EBS to thermal, hydraulic, mechanical, and chemical loading is essential to verify design assumptions and to detect any deviation that could compromise barrier integrity.[6,9] Continuous or repeated monitoring allows changes in key material properties to be identified, supporting both performance assessment and model validation.[11]

In this context, strategies for EBS monitoring typically target a range of bio-thermo-hydro-mechanical and geochemical parameters, including temperature, moisture distribution, porewater pressure, and stress changes.[6] Among these, the evolution of moisture and porewater pressure (water potential or suction) plays a central role, as it directly governs swelling behaviour, hydraulic conductivity, and the overall sealing performance of compacted bentonite buffers.[6,11,12]

The monitoring of volumetric water content and suction can be implemented using different sensing strategies depending on the scale of investigation and the stage of repository development.

During experimental and validation phases, monitoring is commonly carried out in mock-up scale experiments, which are laboratory-scale replicas of EBS, typically ranging from several to tens of centimetres, where local wired sensors can be embedded directly within the barrier material.[13]

Despite the widespread use of TDR, electrical conductivity measurements, and hygrometric techniques in soil physics and geotechnical applications, their applicability to highly compacted bentonite buffers remain insufficiently constrained. In the case of volumetric water content estimation from TDR measurements, the combined effects of high dry density, elevated pore-fluid electrical conductivity, and the presence

* Correspondence to: Department of Civil and Environmental Engineering, University of Strathclyde, James Weir Building, Glasgow G1 1XJ, UK.
E-mail address: alessandro.tarantino@strath.ac.uk (A. Tarantino).

https://doi.org/10.1016/j.gete.2026.100855
Received 4 June 2025; Received in revised form 11 June 2026; Accepted 17 June 2026
Available online 19 June 2026
2352-3808/© 2026 The Author(s). Published by Elsevier Ltd. This is an open access article under the CC BY license (http://creativecommons.org/licenses/by/4.0/).

of adsorbed water challenge the validity of conventional empirical relationships.

While such instrumentation is suitable for controlled experiments, the use of wired sensors inside the buffer is not considered viable for future nuclear waste repositories. Wiring may compromise the integrity of the barrier system and can degrade over time due to corrosion, potentially leading to sensor failure.[11,14] At the repository scale, where direct access to the EBS is inherently limited, monitoring is therefore expected to rely predominantly on wireless or non-intrusive approaches.[10,14]

In this context, electrical and electromagnetic geophysical techniques represent one of the viable options for tracking remotely the hydro-mechanical state of the barrier during the operational phase.[15] Battery-powered MEMS sensors with extended wireless data transmission capabilities also represent a possible option.

However, differences between electrical conductivity measurements obtained using high-frequency (TDR-based) techniques in mock-up scale experiment and low-frequency (direct current) techniques in field monitoring remain poorly understood in the context of bentonite. Finally, while relative humidity–based techniques offer a practical route to quantify total suction over the wide range encountered in bentonite buffers, the performance of miniaturised hygrometric sensors under such conditions has not yet been systematically assessed.

Against this background, the present study investigates experimental techniques to characterise the hydro-geo-electrical behaviour of compacted bentonite relevant to Engineered Barrier Systems. Relative dielectric permittivity was measured using commercial TDR probes, to assess their suitability for estimating volumetric water content in electrically conductive, high-density clay materials. Electrical conductivity was independently measured using both TDR and a direct current four-point method to quantify its dependence on volumetric water content and to elucidate the influence of measurement frequency with direct implications for the calibration and interpretation of ERT monitoring; the effect of temperature on electrical conductivity was investigated using the four-point method only. In parallel, total suction was determined using encapsulated MEMS relative humidity sensors and benchmarked against a chilled-mirror dew point psychrometer to evaluate their accuracy and robustness for laboratory and validation-scale experiments. Together, these investigations aim to establish a consistent experimental framework linking dielectric, electrical, and hygrometric measurements to the key state variables governing bentonite buffer behaviour. The results presented in this study underpin the interpretation of measurements obtained in a mock-up scale experiment presented in a companion paper,[16] where Electrical Resistivity Tomography is evaluated for assessing the hydro-geophysical response of engineered barrier systems relevant to nuclear waste repositories.

2. Background

At the mock-up scale, wired sensors are particularly valuable for validating the EBS concept and for developing and calibrating monitoring methodologies. Volumetric water content is commonly measured using relative dielectric permittivity-based techniques, i.e., Time Domain Reflectometry (TDR) and capacitive probes.[12] However, measurements in highly compacted bentonite pose specific challenges that distinguish them from applications in mineral agricultural soils.

In bentonite, the apparent relative dielectric permittivity measured by TDR probes is strongly affected by the high electrical conductivity of the pore fluid. Mojid et al.[17] and Kupfer et al.[18] demonstrated that this effect can significantly distort the measured signal, such that the apparent dielectric permittivity requires a correction for the influence of bulk electrical conductivity (EC) and electromagnetic signal frequency in order to recover the real part of the dielectric permittivity that is genuinely dependent on soil water content.

In addition, the relationship between volumetric water content and (apparent) relative dielectric permittivity in compacted bentonite is more complex than that captured by traditional empirical calibration models. Widely used models proposed by Topp et al.[19] and Ledieu et al.[20] were developed for electrically non-conductive 'mineral' soils within a relatively narrow range of dry density, ρ_d (e.g., ρ_d=1.25 ± 0.15 Mg/m^3 and ρ_d=1.28 ± 0.1 Mg/m^3, respectively). In contrast, compacted bentonite buffers typically exhibit significantly higher dry densities, which leads to higher apparent relative dielectric permittivity at the same volumetric water content. As a result, applying these traditional models to bentonite can lead to systematic overestimation of volumetric water content.[21,22]

The presence of adsorbed (bound) water further complicates dielectric measurements in clay-rich materials. At a given total volumetric water content, adsorbed water reduces the apparent dielectric permittivity relative to that of mineral soil,[23,24] necessitating calibration approaches that explicitly account for the bound fraction. The influence of adsorbed water is also reflected in the temperature dependence of dielectric permittivity in clays, which has been observed to increase with temperature,[25,26] a trend commonly attributed to the partial release of adsorbed water layers.[25]

Physically based attempts to model these effects include the four-phase mixing model (α-model), originally proposed by Dobson et al.[27] and later refined by Heimovaara et al.[28] Dirksen and Dasberg[23] applied such an approach to clay soils. Although their four-phase mixing model apparently proved inadequate, it should be noted that (i) no correction was applied to the apparent relative dielectric permittivity to account for the effect of soil electrical conductivity and (ii) the layer of adsorbed water was assumed to be constant regardless of bentonite water content. To the authors' knowledge, no physically-based models have been proposed and validated for TDR measurement of volumetric water content in bentonite that account for the combined effects of adsorbed water (with variable thickness), soil dry density, and soil bulk electrical conductivity on the measured apparent relative dielectric permittivity.

From an instrument perspective, soils with high bulk electrical conductivity, such as bentonite clay, can also cause severe attenuation of the TDR signal, leading to partial or complete loss of waveform reflections required to determine relative dielectric permittivity. Rod coatings have been shown to reduce signal attenuation and to preserve the information required to estimate the dielectric constant in highly saline soils.[29–32] Coatings substantially alter the measured permittivity and therefore require dedicated calibration. Alternative approaches based on short probes and frequency-domain analysis have also been proposed by Jones and Or,[33] but their application to compacted bentonite remains limited.

The hydro-mechanical evolution of bentonite buffers is commonly described in terms of water potential, also referred to as suction, which governs swelling, hydraulic conductivity, and saturation processes within the EBS.[34] A wide range of suction values is expected during repository evolution,[35] from very high values immediately after emplacement to values approaching zero upon saturation by the surrounding groundwater.

Several experimental approaches are available to quantify water potential, including liquid-based techniques (e.g. tensiometers and axis-translation methods), solid-based methods (e.g. filter paper), and vapour-based techniques relying on relative humidity (RH) measurements (e.g. chilled-mirror dew point psychrometers).[36] However, not all of these methods are suitable for continuous or in-situ monitoring of compacted bentonite barriers. For example, chilled-mirror dew point psychrometers provide accurate measurements over a wide suction range, particularly at high suctions, but require discrete sampling and laboratory testing, and therefore cannot be deployed as embedded sensors within an EBS.

Vapour-based methods are particularly suited to bentonite, as they allow coverage of the very high suction range[37] relevant to early repository stages. In recent years, Micro-Electro-Mechanical Systems (MEMS) relative humidity sensors have become commercially available, offering compact, low-power requirement, low-cost devices[38–40] that

can be integrated into laboratory and mock-up scale experiments. While these sensors provide an attractive alternative to conventional hygrometric techniques, their application to suction measurement in compacted bentonite requires careful assessment in terms of calibration accuracy, measurement stability after equilibration, and consistency with established reference techniques. If proven reliable under such conditions, these sensors could form the basis for future monitoring solutions, provided that appropriate adaptation is undertaken to enable wireless operation and long-term deployment.

Beyond local measurements, electrical and electromagnetic geophysical methods such as Electrical Resistivity Tomography (ERT) offer the potential for non-intrusive monitoring of EBS during the operational phase[24]. The successful interpretation of ERT data relies on robust relationships between electrical resistivity (electrical conductivity), volumetric water content, temperature, and saturation state.

Electrical and geoelectrical measurements have been extensively applied in soils and rocks.[41–45] However, their application to highly compacted bentonite buffers remains challenging due to strong coupling between electrical conductivity, temperature, salinity, degree of saturation, and clay-bound water. Recent advances have been reported by Chen et al.,[46,47] who developed and validated an ERT-based framework for bentonite buffer monitoring within the HotBENT experiment, including a petrophysical relationship adapted from the Waxman–Smits model. While these studies represent a significant step forward, the proposed relationships are recent and rely on material-specific calibration under controlled conditions. Additional experimental characterisation is therefore required to support the interpretation of ERT data across a wide range of conditions relevant to EBS.

In this context, the comparison between high-frequency TDR-derived electrical conductivity and low-frequency direct current (DC) measurements is particularly relevant. Electrical resistivity tomography is fundamentally based on DC measurements, and its successful application requires robust calibration of the relationship between resistivity (conductivity) and volumetric water content. Since TDR probes are already widely used to estimate volumetric water content and can also provide bulk electrical conductivity, assessing their consistency with DC measurements allows evaluating whether TDR could serve as a practical alternative or complement for conductivity–volumetric water content calibration in experimental and monitoring applications.

3. Measurement techniques

This section describes the experimental techniques used to measure the primary physical quantities investigated in this study, namely relative dielectric permittivity, bulk electrical conductivity, and relative humidity. These measurements constitute the basis for the subsequent estimation of volumetric water content and total suction using established empirical and physically based relationships, which are introduced where relevant. The focus here is therefore on the principles and implementation of the measurement techniques themselves.

3.1. Volumetric water content measurement

TDR probes manufactured by Campbell Scientific (CS640, 75 mm long rods, Fig. 1a) were used for the measurement of volumetric water content (θ_w) through the measurement of the apparent relative dielectric permittivity inferred from the TDR reflection waveform. The TDR probe was first calibrated in air and demineralised water following the procedure described by Tarantino et al.[48] to derive i) the time at which the wave leaves the probe head and enter the probe electrodes (t_{probe}) and ii) the electrical length of the waveguide, L. The sample's apparent relative dielectric permittivity, K_a, was then obtained from the propagation velocity of the pulse in the probe:

$$K_a = \left(c\frac{\Delta t}{2L}\right)^2 \quad (1)$$

where c is the velocity of the electromagnetic signal in free space (3×10^8 m/s), Δt is the time for the pulse to travel forward and backward the length of the embedded waveguide ($\Delta t = t_{end} - t_{probe}$ and $t_{probe} = t_{head} + \Delta t$, Fig. 1*b*) t_{end} is the time marking the reflection at the probe rod end and t_{head} is the time at which the wave enters the probe (Tarantino et al.[48]).

3.1.1. Traditional empirical equations

In the first instance, the apparent relative dielectric permittivity measured by TDR was converted into volumetric water content using commonly adopted empirical calibration equations. These relationships are presented here to provide a reference against which more physically based approaches can be evaluated.

Thus, the volumetric water content was inferred from the apparent relative dielectric permittivity via the empirical equations proposed by Topp et al.[19] and Ledieu et al.[20] respectively and routinely used in TDR volumetric water content measurements:

$$\theta_w = -5.3 \times 10^{-2} + 2.92 \times 10^{-2} \times K_a - 5.5 \times 10^{-4} \times K_a^2 + 4.3 \times 10^{-6} \times K_a^3 \quad (2)$$

$$\theta_w = 0.1138 \times \sqrt{K_a} - 0.1758 \quad (3)$$

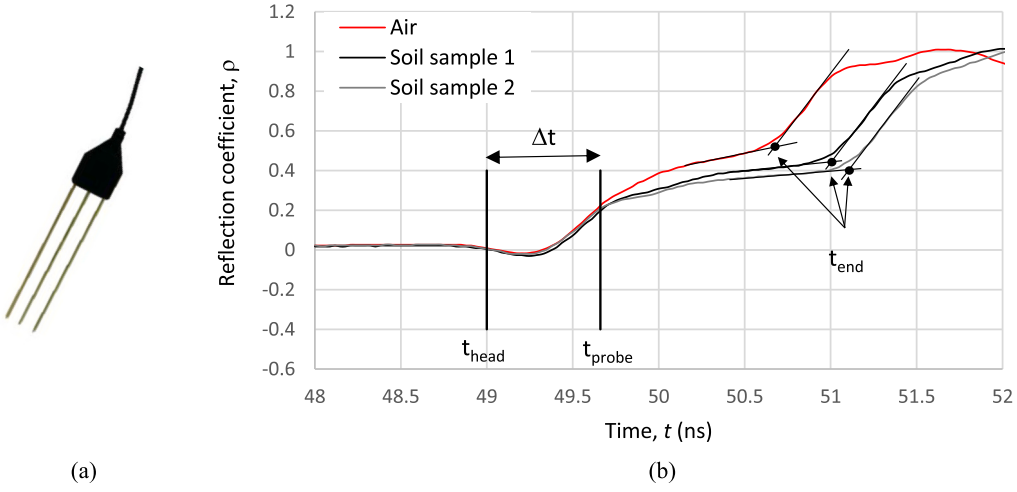

(a) (b)

Fig. 1. (a) TDR CS640 Campbell Scientific (b) Illustration of graphical determination of t_{head}, t_{probe}, t_{end} and Δt for probe in air and distinct soil samples.

To account for the relatively low density of samples compacted at high volumetric water content, the empirical equation proposed by Malicki et al.[49] was also considered:

$$\theta_w = \frac{\sqrt{K_a} - 0.819 - 0.168\rho_d - 0.159\rho_d^2}{7.17 + 1.18\rho_d} \quad (4)$$

where ρ_d is the dry density (Mg/m^3).

At sufficiently high electrical conductivity, signal attenuation may prevent the identification of the reflection at the probe rod end, in which case the apparent relative dielectric permittivity cannot be reliably determined from the TDR waveform.

3.1.2. Four-phase mixing model with dielectric permittivity correction for electrical conductivity

In a second instance, a physically based approach was considered to estimate volumetric water content from TDR measurements, in order to overcome the limitations of traditional empirical calibration equations when applied to compacted fine-grained soils.

Empirical relationships such as those proposed by Topp et. al.,[19] Ledieu et al.,[20] and Malicki et al.[49] (Eqs. (2)–(4) respectively) were developed primarily for mineral agricultural soils and do not explicitly account for the effects of pore-fluid electrical conductivity, dry density (except Malicki et al.[49]), or bound water, all of which are significant in bentonite.

In electrically conductive materials, the apparent permittivity K_a is affected by the pore-fluid electrical conductivity. Indeed, the volumetric water content should be associated with the real part of the dielectric permittivity ε'_m rather than the apparent permittivity K_a. Assuming the imaginary part of the dielectric permittivity to be negligible (since the frequency bandwidth is significantly lower than the relaxation frequency of water at ~20 GHz), the real part of the dielectric permittivity is given by Chung and Lin[50]:

$$\varepsilon'_m = K_a - \frac{1}{4K_a}\left(\frac{\sigma_{TDR}}{2\pi f \varepsilon_0}\right)^2 \quad (5)$$

where σ_{TDR} is the electrical conductivity determined from the TDR standing wave and f is the frequency bandwidth. In turn, the frequency bandwidth can be defined by the 10–90% rise time (t_r) of the end reflection as Strickland.[51]

$$f = \frac{\ln(0.9/0.1)}{2\pi t_r} \quad (6)$$

Bentonite clay is characterised by very high specific surface that, in combination with the electrical charge of the particles due to isomorphous substitutions, gives rise to a non-negligible amount of water that is bound to the particles. Bound water has dielectric properties different from the ones of free water and its presence affects the measurement of the apparent dielectric permittivity. Its effect is not accounted for in routine calibration equations (Eqs. (2)–(4)) developed and calibrated for mineral soils. In order to account for the effect of bound water as well as the effect of dry density on the relationship between the volumetric water content and the (real part of) the dielectric permittivity of the mixture, the following mixing model can be considered:[48]

$$\sqrt{\varepsilon'_m} = \frac{V_s}{V}\sqrt{\varepsilon_s} + \frac{V_a}{V}\sqrt{\varepsilon_a} + \frac{V_{fw}}{V}\sqrt{\varepsilon_{fw}} + \frac{V_{bw}}{V}\sqrt{\varepsilon_{bw}} \quad (7)$$

where V_s, V_a, V_{fw}, and V_{bw} are the volumes of the solids, air, free water, and bound water respectively, V is the total volume of the mixture, and ε_s, ε_a, ε_{fw}, and ε_{bw} are the values of dielectric permittivity of the solids, air, free water, and bound water respectively. The volume fractions in Eq. (7) can be expressed in terms of phase relationship as follows:

$$\frac{V_{fw}}{V} = \theta_{fw}$$

$$\frac{V_{bw}}{V} = \theta_{bw}$$

$$\frac{V_s}{V} = \frac{\rho_d}{\rho_s}$$

$$\frac{V_a}{V} = 1 - \frac{\rho_d}{\rho_s} - \theta_w \quad (8)$$

where θ_{fw} and θ_{bw} are the volumetric water contents of the free water and bound water respectively, ρ_d is the dry density, ρ_s is the density of the solids, and θ_w is the volumetric water content $(\theta_w = \theta_{fw} + \theta_{bw})$.

In turn, the volumetric water content of the bound water θ_{bw} can be assumed to be proportional to the volumetric water content according to Rhoades et al.[52]:

$$\theta_{bw} = \chi\theta_w \quad (9)$$

This equation is valid only in the range where the volumetric water content of free water, θ_{fw} is greater than zero; that is, it does not apply in the range where water is held solely hygroscopically. The bound water is associated with the water in the electrical diffuse double layer. At low volumetric total water contents, the free water would be characterised by high electrolyte concentration that, in turn, would cause the thickness of the double layer (Debye length) to be very small. At high volumetric total water contents, the diluted free water would cause the double layer to expand with the volumetric water content of the bound water increasing accordingly. This effect is qualitatively captured by Eq. (9)

By combining Eqs. (7)–(9), the following calibration equation can be derived:

$$\theta_w = \frac{\left(\sqrt{\varepsilon_s} - \sqrt{\varepsilon_a}\right)\frac{\rho_d}{\rho_s} + \sqrt{\varepsilon_a} - \sqrt{\varepsilon'_m}}{\sqrt{\varepsilon_a} - (1-\chi)\sqrt{\varepsilon_{fw}} - \chi\sqrt{\varepsilon_{bw}}} \quad (10)$$

The parameter χ was estimated by best fitting using the least-square method (χ=0.109) assuming ε_a= 1, ε_s= 4, ε_{bw}= 4, and ε_{fw}= 80. The value ε_{bw} = 4 was adopted following Friedman,[53] who suggested that the high-frequency permittivity of water molecules bound to mineral surfaces can be approximated by the high-frequency permittivity of free water, which lies in the range 4–5.[54]

3.2. Electrical conductivity measurement

3.2.1. TDR standing wave

This procedure enables bulk electrical conductivity (σ) to be determined directly from the steady-state TDR response, independently of the relative dielectric permittivity measurement derived from the reflection travel time.

The TDR determination of electrical conductivity is based on the reflection coefficient at infinite time, ρ_∞, obtained from the standing wave. For calibration purposes, the reflection coefficient at infinite time was also measured with the probe in air and under short-circuit conditions, denoted ρ_{air} and ρ_{sc} respectively (Fig. 2). These reference values were then used to derive the corrected reflection coefficient, $\rho_{\infty,corr}$ (Tarantino et al.[48]):

$$\rho_{\infty,corr} = 1 + 2\frac{\rho_{air} - \rho_\infty}{\rho_\infty - \rho_{sc}} \quad (11)$$

The calibration curve allowing inferring the bulk electrical conductivity from the corrected reflection coefficient recorded at infinite time, $\rho_{\infty,corr}$, was derived by immersing the TDR probe in NaCl solutions of known concentration. This allowed deriving the slope K_p/Z_c of the calibration curve.[48]

$$\rho = \frac{K_p}{Z_c}\left[\frac{1 + \rho_{\infty,corr}}{1 - \rho_{\infty,corr}}\right] \quad (12)$$

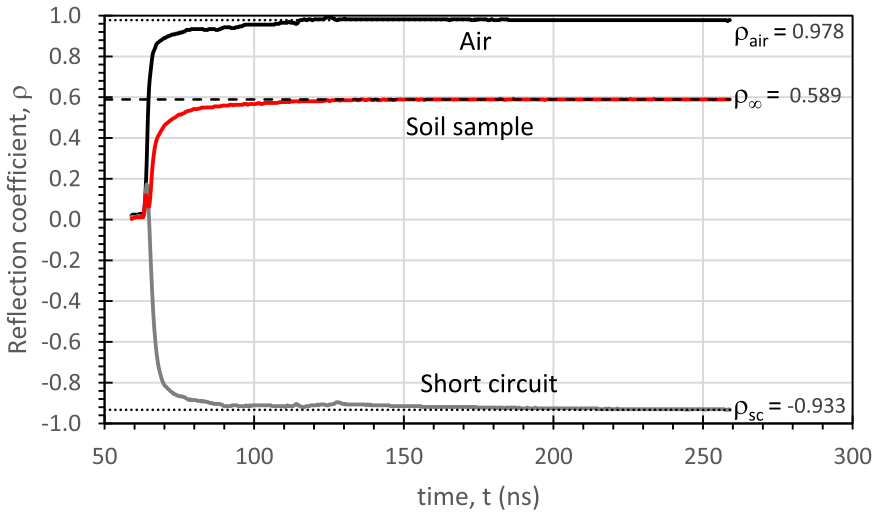

Fig. 2. Illustration of graphical determination of ρ_{∞} for a soil sample, ρ_{air} and ρ_{sc} for probe in air and short circuited, respectively.

where K_p is the probe constant and Z_c is the impedance of the cable tester (Z_c/K_p=0,118 S/m)

3.2.2. Direct Current (DC) four-point method

The direct current (DC) four-point method is a standard technique for measuring bulk electrical conductivity under low-frequency (quasi-static) conditions. The method consists in injecting a current through electrodes located at the ends of a cylindrical sample holder, while the resulting electrical potential difference is measured between two inner electrodes (Fig. 3). The current electrode disks were made of copper with diameter equal to the diameter of the sample (3 cm) whereas the potential electrodes were made of bronze. The PVC sample holder was 12 cm long and 3 cm in diameter returning a ratio between length and diameter of 4, which is greater than 2.5 as suggested in the literature for unidimensional tests.[55–57] The potential electrodes were installed 10 cm apart (Fig. 3).

3.2.3. Frequency range considerations

The two electrical conductivity measurement techniques employed in this study operate over markedly different frequency ranges, which may influence the measured values. The TDR method operates in the GHz frequency range, whereas the four-point method applies a very low-frequency electrical signal (below 50 Hz) and can therefore be regarded as a direct-current technique. Owing to this difference, the two methods may prove distinct conduction mechanisms within the material. In particular, it is assumed that the high-frequency TDR signal does not effectively mobilise electrical conduction associated with bound water in the diffuse double layer, whereas such contributions may be captured by the low-frequency four-point method. The implications of these frequency-dependent effects on the measured electrical conductivity are examined in the Discussion section.

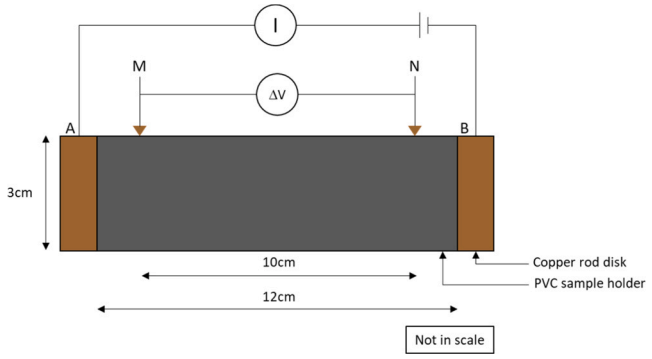

Fig. 3. Schematics of sample holder of geo-electrical characterisation.

3.3. Total suction measurement

Three main categories of techniques are commonly used to measure suction (water potential), depending on the phase of the sensing medium: solid-based methods (e.g., filter paper), liquid-based methods (e.g., tensiometers and axis-translation techniques), and vapour-based methods (e.g., hygrometers).[36]

Hygrometric techniques determine suction by measuring the vapour pressure of water in air, typically expressed as relative humidity (RH). When a soil sample is allowed to equilibrate thermally with the surrounding air, the vapour phase reaches equilibrium with the pore water, enabling RH to be related to total water potential through thermodynamic principles. In this context, equilibrium is established between the liquid water stored in the soil matrix and the water vapour present in the pore space. While humidity describes the absolute amount of water vapour in air, relative humidity corresponds to the ratio of the actual vapour pressure to the saturation vapour pressure at a given temperature. Under equilibrium conditions and a defined reference state, this relationship is formally described by the Kelvin equation.[58]

$$s_T = -\frac{RT}{v_{\omega 0}\omega_v}\ln\left(\frac{u_v}{u_{v0}}\right) = \frac{RT}{v_{\omega 0}\omega_v}\ln(RH) \tag{13}$$

where s_T is total suction, R is the universal gas constant (8.31432 J·mol^{-1}·K^{-1}), T is the absolute temperature in Kelvin, $\nu_{\omega 0}$ is the specific volume of water, ω_v is the molecular mass of water vapour (18.016 g/mol), and u_v and u_{v0} represent the partial pressure of water vapour and the vapour pressure of water vapour at saturation respectively.

When temperature and relative humidity are known, total suction can be directly calculated using this thermodynamic relationship. Consequently, relative humidity measurements provide an indirect but well-established means of quantifying suction in unsaturated soils and engineered barrier materials.[37]

In recent years, Micro-Electro-Mechanical Systems (MEMS) relative humidity sensors have emerged as a promising alternative to traditional techniques such as chilled-mirror hygrometers and psychrometers. MEMS sensors, owing to their small size, low power consumption, and ease of integration into confined experimental setups.[40]

MEMS RH sensors, including those employed by Yang et al.,[39] typically rely on capacitive or resistive mechanisms where changes in the material properties of the sensor due to moisture absorption result in

variations in the electrical output. These sensors have been shown to provide stable and repeatable measurements of humidity and temperature, making them ideal for continuous estimation of total suction once thermal equilibrium is achieved between the sensor and the soil. Despite these advantages, MEMS sensors require careful calibration, especially under high humidity or temperature gradients, and their long-term performance may be affected by condensation or sensor drift.[59] Nonetheless, their miniaturized form factor and adaptability make MEMS sensors an attractive choice for controlled laboratory experiments, where sensor performance can be rigorously validated, and—if proven reliable—potentially form the basis for future wireless sensing solutions for in situ EBS monitoring.

MEMS sensors (Sensirion® SHT25) were used to measure Relative Humidity. These sensors operate on a capacitive measurement principle, whereby moisture adsorption within a hygroscopic polymer layer induces changes in capacitance that are converted into RH values. The sensor provides simultaneous temperature measurements with an accuracy of ±0.5 °C over the range −55–150 °C, and relative humidity measurements with a nominal accuracy of ±1.8% RH between 10–90% RH and ±3% RH over the full 0–100% RH range.[38] To enhance robustness in bentonite environments, the sensor was protected by a PTFE membrane and encapsulated in polyurethane resin, resulting in a compact sensing unit of approximately 10 × 12 × 3 mm (Fig. 4), as proposed by Yang et al..[38] This configuration allows vapour diffusion while preventing liquid water ingress and mechanical damage.

These sensors were calibrated individually by exposure to six different saturated salt solutions at room temperature (Table 1). Readings were recorded after equilibrium of *RH* inside the containers was achieved, which took around 3 h. *RH* values imposed by salt solutions were derived from Winston and Bates[60] and Greenspan[61] at 20°C. These theoretical values were adjusted according to the temperature recorded by the sensors through relationships obtained from data published in the literature.[60]

Fig. 5 illustrates the measured *RH* against the known *RH* imposed by the salt solution for a sensor. There is excellent agreement between the imposed and measured *RH* values and no correction was therefore required for the *RH* measurement by the MEMS sensors.

To benchmark the *RH* measured by the *RH* sensors, relative humidity was also measured using a chilled-mirror dew point psychrometer (WP4C, Decagon Devices, Inc., Pullman, WA, USA). Although the psychrometer actually measures relative humidity, the measurement is displayed in terms of total suction s_T according to Eq. (13). This equation was used to derive the value of total suction from the relative humidity of the air surrounding the sample.

4. Material and experimental procedures

4.1. Material

The bentonite clay material under investigation is constituted by a mixture of bentonite pellets and powder, prepared and provided by Nagra.[62] This natural sodium bentonite is commercially known as National® Standard, mined by Bentonite Performance Minerals (BPM) in Wyoming.[62] The bentonite clay material, as received, had a gravimetric

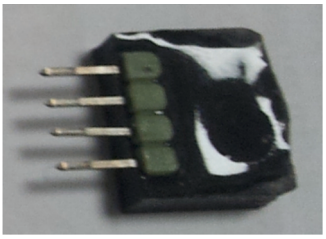

Fig. 4. Encapsulated MEMS sensor.

Table 1
Saturated salts used to calibrate relative humidity sensors.

Salt	Known RH at 20°C (%)
K_2CO_3	43.16
KI	69.90
NaCl	75.47
KCl	85.11
Na_2CO_3	92.00

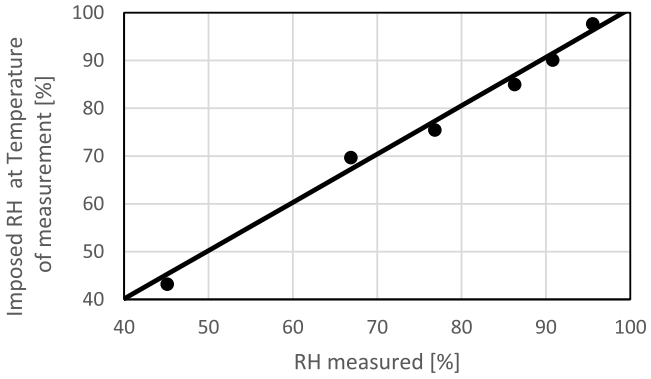

Fig. 5. RH calibration with salt solutions.

water content of 6%. Fig. 6 shows the particle size distribution of the material.

A synthetic water representative of the Callovo-Oxfordian argillite at Bure (France)[63] was used. The chemical composition of the synthetic water is given in Table 2. The conductivity of the water measured with a conductivity probe meter was 0.39 S/m.

4.2. Specimen preparation and measurement procedure

Bentonite clay samples were prepared by manually mixing bentonite clay with synthetic water up to the target gravimetric water content as indicated in Table 3. All samples were left in a sealed bag for 24 h for homogenisation before compaction.

4.2.1. TDR measurements

The material was compacted in an acrylic mould (internal dimensions: 88.2 mm in diameter and 31.0 mm in height). Compaction was carried out up to the mid-height corresponding to the position of the TDR probe, which was then placed in position before compacting the remaining material above it. The specimens were then left to equilibrate for approximately 3 h before measurement. After equilibration, two waveforms were acquired, one with a short window interval (10 ns) to acquire the reflection waveform for the determination of the apparent

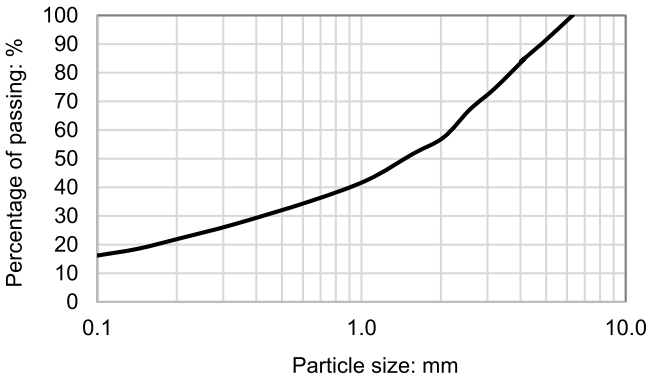

Fig. 6. Particle size distribution of bentonite clay pellets and powder.[62]

Table 2
Chemical composition of synthetic water.

Salt	Molar mass (g/mol)	Concentration (mol/L)
Calcium Sulphate	169.17	7.60E−03
Sodium Hydrogen Carbonate	84.01	4.20E−03
Magnesium Sulphate Heptahydrate	246.47	5.90E−03
Potassium Chloride	74.56	8.99E−04
Sodium Sulphate	142.04	5.50E−03
Sodium Chloride	58.44	4.00E−03

Table 3
Summary of specimen conditions prepared for DC four-point, RH, and TDR measurements at different temperatures.

Specimens prepared for DC four-point method measurements					
Specimens subjected to 70 °C			Specimens subjected to 50 °C		
w before heating	w after heating	Bulk density (Mg/m^3)	w before heating	w after heating	Bulk density (Mg/m^3)
0.18	0.18	1.43	0.19	0.18	1.52
0.24	0.24	1.52	0.24	0.24	1.67
0.28	0.27	1.52	0.27	0.27	1.55
0.30	0.29	1.40	0.32	0.31	1.46
0.39	0.39	1.63	0.39	0.39	1.72
0.45	0.44	1.42	0.44	0.44	1.46
0.58	0.58	1.49	0.59	0.58	1.56
0.71	0.71	1.53	0.73	0.72	1.61
0.85	0.85	1.55	0.88	0.86	1.53
1.00	0.98	1.57	0.98	0.95	1.45
Specimens subjected to 40 °C			Specimens subjected to 30 °C		
w before heating	w after heating	Bulk density (Mg/m^3)	w before heating	w after heating	Bulk density (Mg/m^3)
0.19	0.19	1.59	0.17	0.17	1.59
0.24	0.22	1.63	0.23	0.23	1.51
0.28	0.26	1.50	0.27	0.27	1.53
0.32	0.32	1.49	0.31	0.31	1.52
0.38	0.37	1.68	0.41	0.41	1.61
0.46	0.45	1.61	0.44	0.44	1.62
0.59	0.59	1.69	0.59	0.59	1.69
0.73	0.73	1.66	0.72	0.72	1.64
0.86	0.86	1.62	0.85	0.85	1.56
0.97	0.97	1.55	1.00	0.99	1.57

Specimens prepared for RH (suction) measurements			Specimens prepared for TDR measurements		
w	θ_w	Bulk density (Mg/m^3)	w	θ_w	Bulk density (Mg/m^3)
0.07	0.10	1.46	0.14	0.17	1.45
0.08	0.11	1.45	0.19	0.21	1.45
0.10	0.12	1.47	0.24	0.26	1.45
0.14	0.17	1.45	0.29	0.29	1.41
0.19	0.21	1.45	0.33	0.35	1.42
0.24	0.26	1.45	0.41	0.41	1.39
0.29	0.29	1.41	0.60	0.60	1.47
0.33	0.35	1.42	0.76	0.64	1.39
0.41	0.41	1.39	0.98	0.70	1.39
0.60	0.60	1.47	1.40	0.73	1.41
0.76	0.64	1.39			
0.98	0.70	1.39			
1.40	0.73	1.41			

where: w = gravimetric water content and θ_w: volumetric water content

relative dielectric permittivity K_a (Fig. 1) and a second one with a long window interval (200 ns) to acquire the standing wave for determination of the reflection coefficient at infinite time ρ_∞ (Fig. 2). After acquiring the waveforms, a small specimen was cut and trimmed using a sampler of known volume (3.68 cm^3) for the determination of the volumetric and gravimetric water content by oven-drying.

4.2.2. Direct current four-point method

Samples were compacted into the cylindrical sample holder (Fig. 3) at gravimetric water content and bulk densities shown in Table 3 and the conductivity was recorded at environmental temperature (20°C). The same set of samples were heated in an oven to four temperatures: 30°C, 40°C, 50°C, and 70°C. Temperature was maintained constant for 24 h for each temperature step. The gravimetric water content of each sample was back-calculated after compaction at 20°C and after the heating tests (the difference between gravimetric water content after compaction and after heating showed a mean decrease of 0.006, standard deviation of 0.002). Before and after each temperature level, the loss of weight and the conductivity were measured. The electrical conductivity was recorded immediately after removal from the oven and also 5 h afterwards under thermal equilibrium (sample temperature equilibrated to room temperature) following Cosenza et al..[57]

4.2.3. Relative humidity measurements

Several samples were prepared at different gravimetric water contents (Table 3). The material was compacted in an acrylic mould (internal dimensions: 88.2 mm in diameter and 31.0 mm in height). Compaction was carried out up to the mid-height corresponding to the position of the RH sensor, which was then placed in position before compacting the remaining material above it. The RH was continuously recorded at regular intervals, and the value after equilibration, typically reached within 2–3 h when readings stabilized, was taken as the representative RH measurement.

After measuring the relative humidity, hence total suction, the sample was removed from the acrylic mould and small specimens were cut and trimmed from the large cylindrical sample with the help of a cylindrical metallic cutting-edge sampler (16.7 mm in diameter and 15.9 mm in height) for the determination of the gravimetric water content and degree of saturation. In this way, the Water Retention Curve (WRC) of the bentonite clay material could be determined. A small specimen was also cut from the large cylindrical sample and put into the WP4C Dew Point psychrometer to measure the relative humidity (hence total suction).

5. Results

5.1. Volumetric water content measurements

Fig. 7 shows the reflection waveforms for the 10 specimens tested. It is first noted that the reflection waveforms for the samples at higher volumetric water contents (from 0.6 to 0.73) do not show the rising limb associated with the wave reflection at the probe rod end. This is due to the relatively high electrical conductivity in turn causing the signal to dissipate entirely before reflection occurs at the end of the probe. As a result, higher volumetric water contents cannot be captured by the TDR probes, and a probe coating would have been required to enable measurements at these elevated volumetric water contents.

The reflection waveforms at lower volumetric water contents (0.17–0.41) exhibit a rising limb that becomes progressively gentler as volumetric water content increases. This occurs because the soil becomes more electrically conductive with increasing volumetric water content, which leads to greater dispersion of the electromagnetic signal.

Fig. 8 shows the estimated volumetric water content via Eqs. (2), (3) and (4) versus the measured volumetric water content. The empirical equations by Topp et al.[19] Ledieu et al.[20] (Eqs. (2) and (3) respectively) significantly underestimate the volumetric water content in the low range. The equation by Malicki et al.[49] (Eq. (4)), which accounts for the effect of density, improves the estimation but only marginally. Fig. 8 clearly shows that 'traditional' empirical calibration curves, developed mainly for non-clayey soils, are not adequate to estimate the volumetric water content of highly active clay. Most data points lie well below the

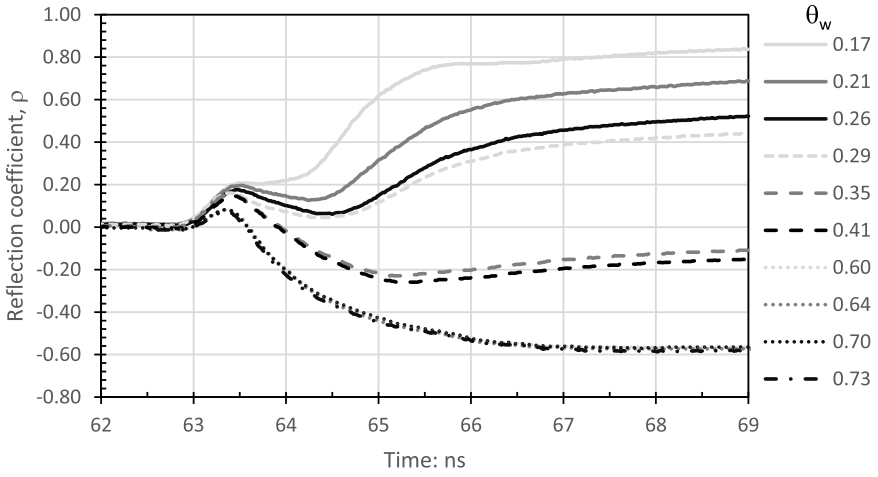

Fig. 7. Reflection waveforms at different measured volumetric water contents.

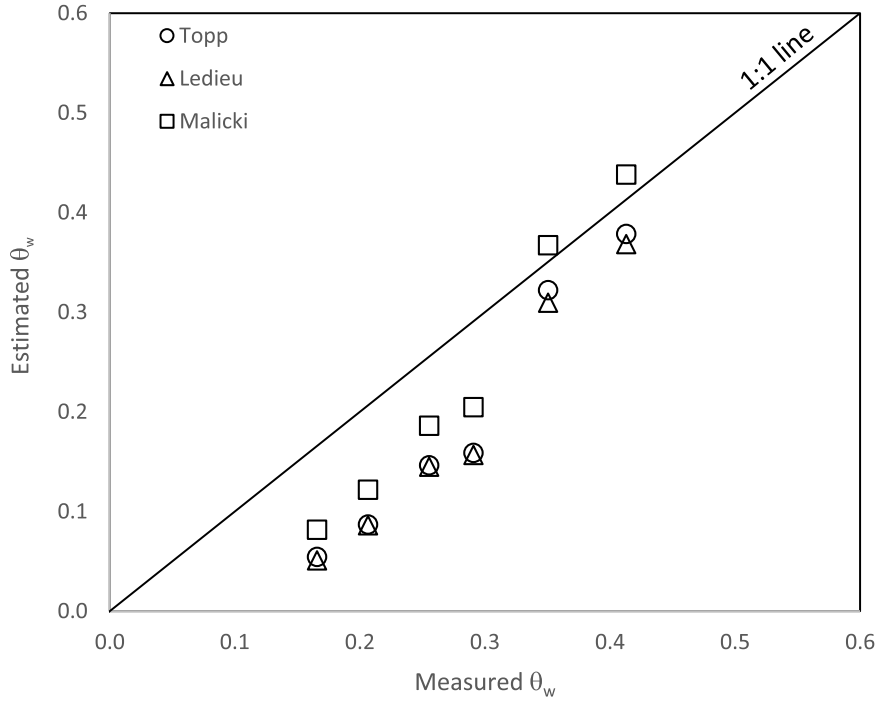

Fig. 8. Estimated versus measured volumetric water content.

1:1 line, indicating a systematic underestimation of volumetric water content over the investigated range.

The volumetric water content was subsequently estimated by replacing the apparent permittivity K_a in Eqs. (2), (3) and (4) with the real part of the dielectric permittivity ε'_m as defined by Eq.(5). The corresponding results are shown in shown in Fig. 9 with rise time and associated frequency bandwidth values reported in Table 4. Although the corrected estimates still deviate from the measured volumetric water contents, the data points tend to align parallel to the 1:1 line, suggesting the presence of a systematic offset affecting the estimation.

Fig. 10 presents the volumetric water content estimated using the four-phase mixing model (Eq. (10)), which accounts for dry density, pore-fluid electrical conductivity, and bound water effects. The results demonstrate a marked improvement in the agreement between estimated and measured volumetric water contents. These findings indicate that volumetric water content in compacted bentonite can be successfully estimated from TDR measurements provided that the effects of: i) the relatively higher dry densities typically encountered in compacted soils compared with the agricultural soils used to derive traditional models, ii) pore-fluid electrical conductivity on the measurement of apparent relative dielectric permittivity, and iii) significant amounts of bound water, are explicitly accounted for.

5.2. Electrical conductivity measurement

The relationship between electrical conductivity determined via TDR probes and the measured volumetric water content is presented in Fig. 11. The TDR electrical conductivity increases with the volumetric water content as expected. The same trend is observed for the electrical conductivity measured via the four-point method (Fig. 11). However, there is appreciable difference between the two methods, with four-point method returning systematically higher values of electrical conductivity. Although TDR and four-point method conductivity are both used to measure soil electrical conductivity, we found no direct, side-by-

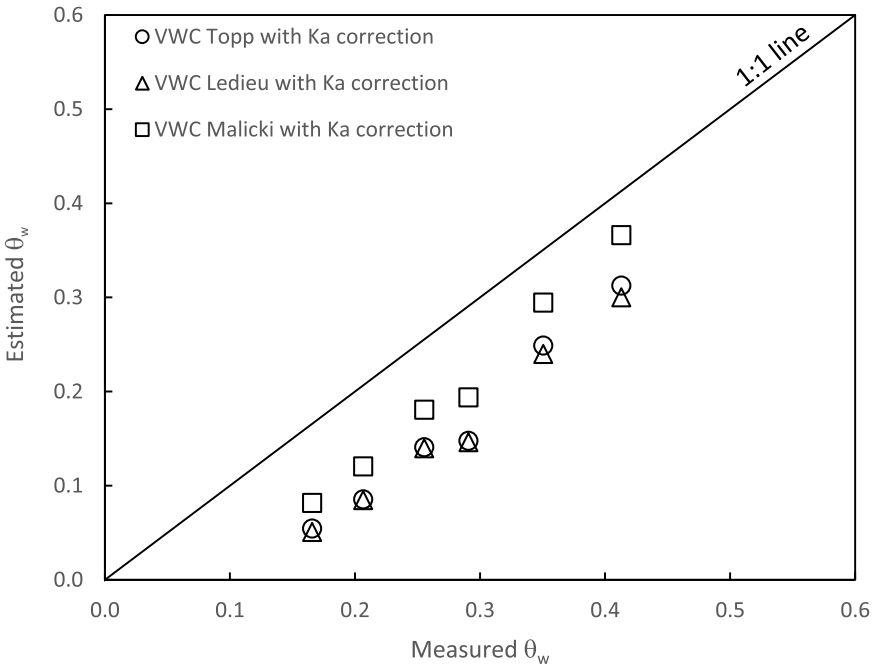

Fig. 9. Estimation of volumetric water content θ_w after correcting the apparent permittivity K_a.

Table 4
Rise time, t_r, and frequency, f, bandwidth associated with the reflection waveforms shown in Fig. 7.

θ_w	0.17	0.21	0.26	0.29	0.35	0.41
t_r [ns]	1.02	2.9	2.8	2.75	2.68	2.9
f [GHz]	0.343	0.121	0.125	0.127	0.131	0.121

side comparisons of these two methods in the same soils and conditions. Related work has validated TDR against alternate current (AC) conductivity bridges measuring electrical conductivity in a frequency range of 1–20 kHz, which is much higher than the frequency used in the four-point method (<50 Hz).[64] An interpretation of this discrepancy is provided later in the paper.

5.3. Relative humidity measurement

Fig. 12 shows the *RH* measured by the MEMS sensors 'sandwiched' in different bentonite samples against the *RH* measured post-mortem on specimens cut from the bentonite samples via WP4C equipment. There appears to be an excellent agreement between the two measurements showing the MEMS sensors are reliable devices to be used in mock-up or full-scale experiments for validating EBS concepts.

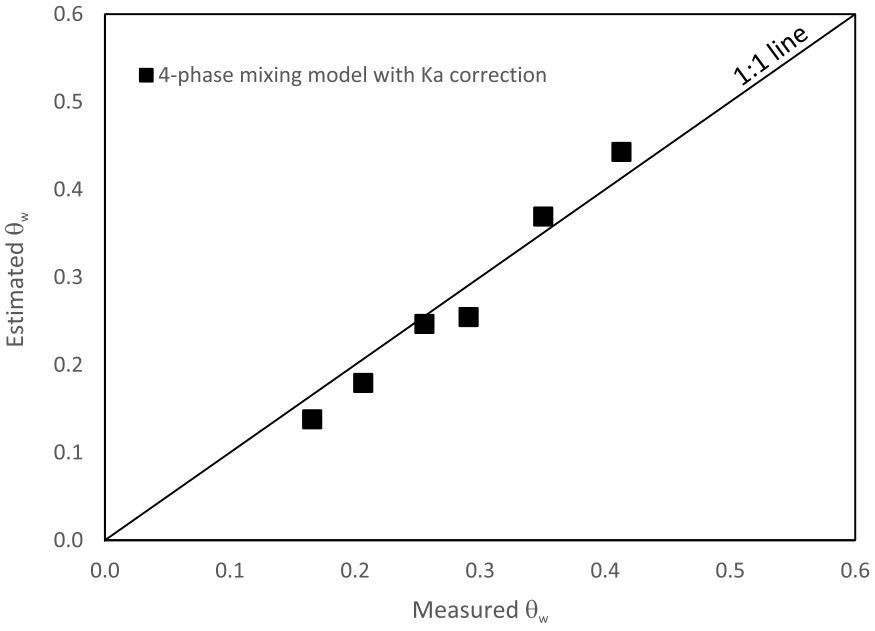

Fig. 10. Estimation of volumetric water content θ_w using the 4-phase mixing model (with correction of apparent permittivity K_a).

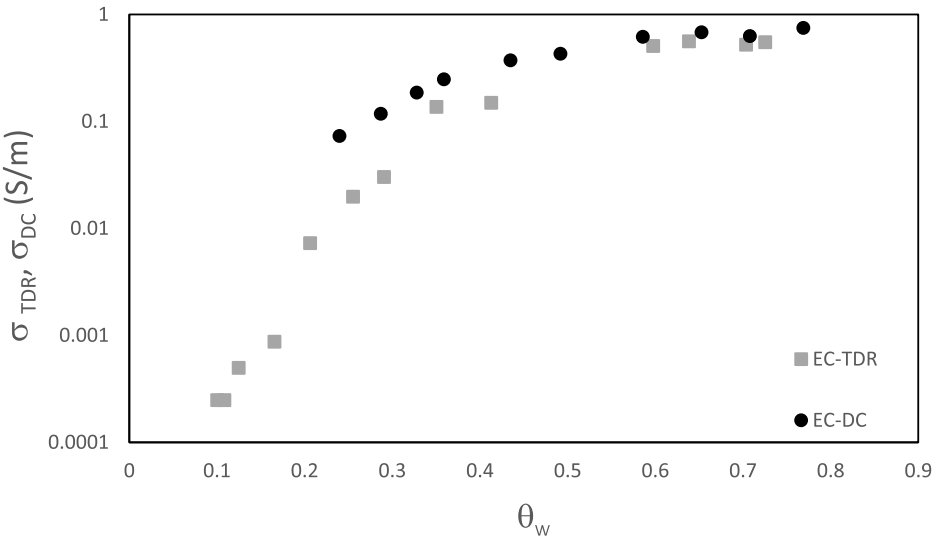

Fig. 11. Electrical conductivity measured via TDR (EC-TDR) and direct current four-point method (EC-DC).

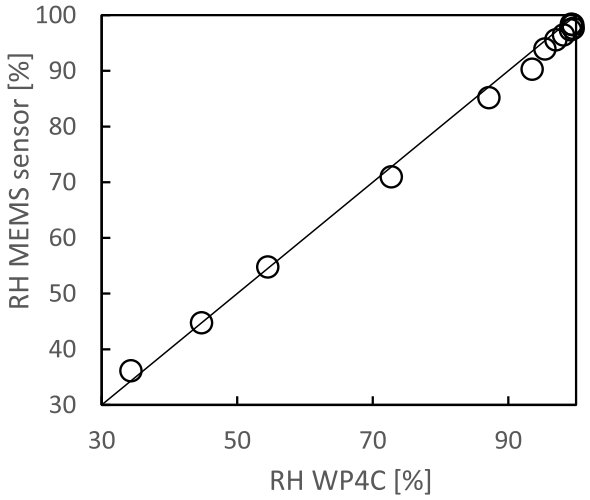

Fig. 12. Bentonite samples – RH comparison between MEMS sensors and WP4C device.

5.4. Hydraulic and geo-electrical characterisation

The water retention curve in terms of degree of saturation S_r versus suction s is presented in Fig. 13. The series shown in the graph were fitted through the correlation proposed by Gallipoli et al.,[65] who adapted the van Genuchten equation[66] to include the dependency of water retention behaviour on void ratio.

$$S_r = \left[\frac{1}{1+(\phi e^{\psi} s)^n}\right]^m \tag{14}$$

where ϕ, ψ, m and n are soil constants that describes the soil's water retention behaviour, defining shape, curvature, and deformation sensitivity of the curve. The fitting parameters used for the bentonite material are: $\phi = 8.06 \times 10^{-4}$ kPa^{-1}, ψ= 0.952, m = 0.112 and n = 2.973.

The effect of void ratio is shown by plotting the curves associated with void ratios of e= 0.9 and e= 1.4 respectively and the data falling in the range e= 0.9 ± 0.3 and e= 1.4 ± 0.2 respectively, which reflect the variability in void ratio observed among samples prepared at different gravimetric water contents.

Fig. 14 shows the effect of temperature on the relationship between volumetric water content and electrical conductivity measured via the four-point method. The data are presented in terms of difference between the electrical conductivity at the temperature T and the electrical conductivity at T = 20°C. This difference increases as the temperature increases and amplifies at higher volumetric water contents.

The observed increase in electrical conductivity with temperature is consistent with previously reported findings.[67] The bulk electrical conductivity of soils is governed by two primary mechanisms: pore water

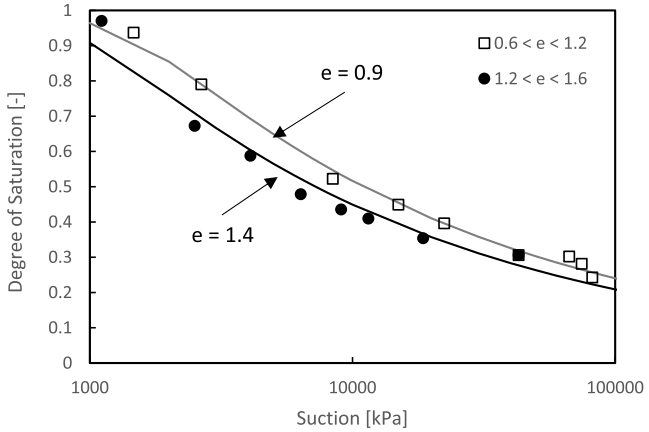

Fig. 13. Water Retention curves of Bentonite clay material.

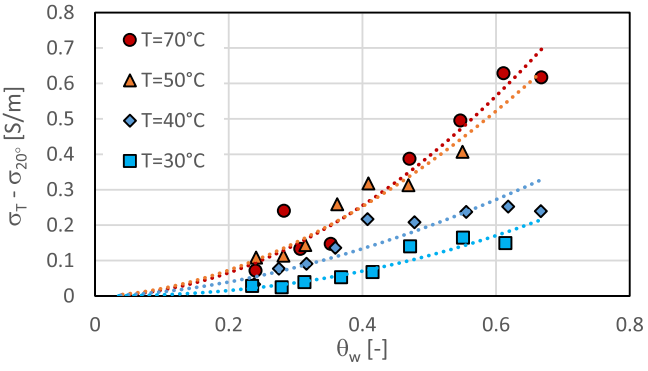

Fig. 14. Difference in electrical conductivity measured immediately after oven treatment and after temperature equilibration at 20°C, where dotted lines are power-law fitted curves.

conduction (K_w), which represents ionic conduction through the interconnected pore space, and surface conduction (K_s), which is associated with ionic movement within the diffuse double layer surrounding soil particles. Both K_w and K_s increase with temperature. However, their underlying mechanisms differ. K_w increases primarily because the viscosity of pore water decreases with temperature, allowing ions to move more freely, while Ks increases because higher temperatures enhance cation mobility in the diffuse double layer.

As a result, soil electrical conductivity typically increases by approximately 2% per 1 °C rise in temperature.[68–73] However, for materials dominated by surface conduction, such as bentonite, the temperature dependency tends to be lower.[74] The surface conductivity of bentonite increases non-uniformly with temperature and exhibits lower temperature sensitivity than that typically observed in mineral soils, due to the distinct contribution of the diffuse double layer.[74]

The effect of temperature appears to be of the same order of magnitude as the effect of volumetric water content (see Fig. 11) and this may pose a problem in the interpretation of ERT electrical conductivity data as an increase in electrical conductivity can be due to either an increase in temperature or an increase in volumetric water content in the buffer of the Engineered Barrier System.

6. Discussion

The discrepancies observed between electrical conductivity measurements obtained using TDR and the DC four-point method (Fig. 11) can be interpreted in light of the different frequency ranges at which the two techniques operate, as outlined in 3.2.3.

While TDR measurements are performed in the GHz range, the four-point method operates at very low frequencies and can be regarded as a direct-current technique. As a consequence, the two methods are sensitive to different electrical conduction mechanisms within the bentonite. In particular, the high-frequency TDR signal is unlikely to mobilise electrical conduction associated with bound water in the diffuse double layer, whereas such contributions are captured by the low-frequency four-point measurements. This aligns with experimental evidence presented by Saarenketo[75] showing that, at low water content, electrical conductivity decreases as frequency increases. According to Leroy et al.,[76] the electrical conductivity of bound water is associated with electrical diffuse layer at the outer surface and the interlayer space. This would explain the difference observed in Fig. 11. To corroborate this assumption, the experimental data were modelled using a modified Archie's law for two conducting phases, free water, and bound water respectively. If the electrical conductivity is assumed to be controlled 'in parallel' by electrical conductivities of the bound and free waters,[52] we can write.

$$\sigma = \theta_{fw}\sigma_{fw} + \theta_{bw}\sigma_{bw} \tag{15}$$

where θ_{fw} and θ_{bw} are the volumetric water contents of free and bound water respectively and σ_{fw} and σ_{bw} the electrical conductivities of free and bound water respectively. In turn, the electrical conductivities of free and bound water can be expressed as a power function of volumetric water contents of free and bound water respectively in line with the empirical Archie's law for two-phase porous materials:

$$\sigma_{fw} = a_{fw}\theta_{fw}^{m_{fw}}$$

$$\sigma_{bw} = a_{bw}\theta_{bw}^{m_{bw}} \tag{16}$$

where a_{fw} and m_{fw} are the parameters associated with the free water and a_{bw} and m_{bw} the parameters associated with the bound water. Combination of Eqs. (9), (15) and (16) leads to

$$\sigma = \underbrace{a_{fw}(1-\chi)^{m_{fw}-1}\theta_w^{m_{fw}-1}}_{free\ water} + \underbrace{a_{bw}\chi^{m_{bw}-1}\theta_w^{m_{bw}-1}}_{bound\ water} \tag{17}$$

This is in line with the equation proposed by Glover et al.[77] for two conducting phases and by Van Loon and Mibus[78] for argillaceous rocks even though the authors did not provide a physically-based justification for the use of two distinct terms on the right-hand side of Eq. (17).

The assumption made here is the electrical conductivity measured by the TDR is only associated with the presence of free water

$$\sigma_{TDR} = a_{fw}\theta_w^{m_{fw}} = a_{fw}(1-\chi)^{m_{fw}-1}\theta_w^{m_{fw}-1} \tag{18}$$

that is the first term on the right-hand side in Eq. (17). The parameters a_{fw} and m_{fw} were then derived by best fitting the TDR electrical conductivity data using Eq. (18) as shown in Fig. 15 and Table 5.

On the other hand, the electrical conductivity measured by the four-point method was associated with the presence of both free water and bound water, that is

$$\sigma_{DC} = a_{fw}(1-\chi)^{m_{fw}-1}\theta_w^{m_{fw}-1} + a_{bw}\chi^{m_{bw}-1}\theta_w^{m_{bw}-1} \tag{19}$$

Accordingly, the parameters a_{bw} and m_{bw} were derived by best fitting the four-point method (DC) electrical conductivity data using Eq. (19) as shown in Fig. 15 and Table 5.

The values of the parameters ($m_{fw}-1$) and ($m_{bw}-1$) are in line with the parameters m_1 and m_2 reported by Van Loon and Mibus.[79] This corroborates the assumption the bound water and free water are contributing separately (and in parallel) to the total electrical conductivity.

7. Conclusions

This paper has investigated experimental techniques for measuring volumetric water content, total suction, and electrical conductivity of bentonite-based materials used in the Swiss concept of the geological disposal of nuclear waste.

Within the scope of this research, the relative humidity measured using MEMS sensors and the WP4C are in excellent agreement. Since relative humidity was used to infer total suction through the Kelvin equation, these results demonstrate that MEMS sensors are reliable devices for total suction measurements in mock-up experiments aimed at validating the EBS concept. Therefore these sensors could also form the basis for future water potential monitoring in EBS, provided that appropriate adaptation is undertaken to enable wireless operation and long-term deployment.

The findings also suggest that TDR probes may be used to monitor volumetric water content, provided the calibration equation is reformulated by i) correcting the measured apparent relative dielectric permittivity for the effect of clay electrical conductivity and ii) accounting for the effect of bulk density and adsorbed water. These effects are not accounted for in the traditional Topp's and Ledieu's equations. Electrical conductivity inferred from TDR and direct current four-point method measurements was shown to differ substantially, and such a difference was associated with the frequency-dependent contribution of free and adsorbed water to bulk electrical conductivity. In particular, the high-frequency TDR measurements appear to be governed predominantly by the conductivity of free water, whereas the low-frequency direct current measurements capture contributions from both free and bound water within the diffuse double layer.

This study further demonstrated that the relationship between volumetric water content and electrical conductivity is markedly affected by temperature changes. Overall, this research provides valuable insights into the performance of bentonite clay as an engineered barrier material in nuclear waste repository and highlights the importance of accounting for various factors when monitoring the response of EBS to thermal and hydraulic loading.

CRediT authorship contribution statement

Bruna de Carvalho Faria Lima Lopes: Writing – original draft,

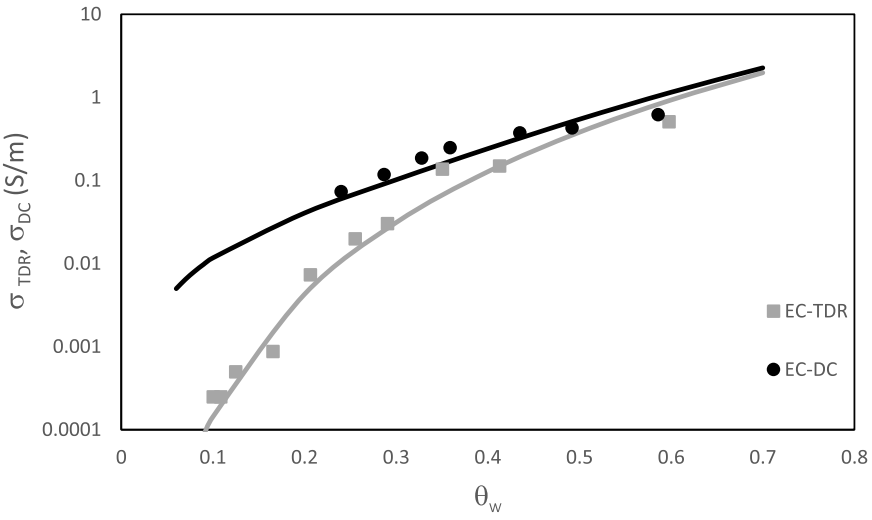

Fig. 15. Modelling electrical conductivity using a two-phase 'in-parallel' mixing model.

Table 5
Parameters of electrical conductivity mixing model.

a_{fw} [S/m]	m_{fw} [-]	a_{bw} [S/m]	m_{bw} [-]	χ^* [-]
20	5.9	20	2.65	0.109

* Calibrated against TDR volumetric water content measurements

Visualization, Validation, Software, Methodology, Investigation, Formal analysis, Data curation, Conceptualization. **Alessandro Tarantino:** Writing – review & editing, Visualization, Validation, Supervision, Resources, Project administration, Investigation, Funding acquisition, Conceptualization.

Funding

This work was supported by the European Commission via the project MODERN2020 'Development and Demonstration of Monitoring Strategies and Technologies for Geological Disposal' (Grant Agreement No. 662177-Modern2020- NFRP−2014–2015) under the H2020 Euratom Research and Training Programme (Funding agency ID: http://doi.org/10.13039/100010687).

Declaration of Competing Interest

The authors declare the following financial interests/personal relationships which may be considered as potential competing interests: Bruna de Carvalho Faria Lima Lopes reports financial support was provided by European Commission. If there are other authors, they declare that they have no known competing financial interests or personal relationships that could have appeared to influence the work reported in this paper.

Acknowledgements

The authors would like to thank NAGRA for providing the Bentonite Clay material for this research and Mr Derek McNee for the laboratory support.

Data availability

Data will be made available on request.

References

1. Levasseur S, Sillen X, Marschall P, et al. EURAD GAS and HITEC: mechanistic understanding of gas and heat transport in clay-based materials for radioactive waste geological disposal. *EPJ Nucl Sci Technol*. 2022;8:21. https://doi.org/10.1051/epjn/2022021.
2. Yim MS. Nuclear waste management. *Lect Notes Energy*. 2022;83:385–459. https://doi.org/10.1007/978-94-024-2106-4_9.
3. Marsh AI, Williams LG, Lawrence JA. The important role and performance of engineered barriers in a UK geological disposal facility for higher activity radioactive waste. *Prog Nucl Energy*. 2021;137(January), 103736. https://doi.org/10.1016/j.pnucene.2021.103736.
4. Bredehoeft JD, England AW, Stewart DB, Trask NJ, Winograd IJ. *Geologic disposal of high-level radioactive wastes- Earth-science perspectives*. 1978.
5. Ojovan MI, Steinmetz HJ. Approaches to disposal of nuclear waste. *Energies*. 2022;15(20). https://doi.org/10.3390/en15207804.
6. Sellin P, Leupin OX. The use of clay as an engineered barrier in radioactive-waste management - a review. *Clays Clay Miner*. 2014;61(6):477–498. https://doi.org/10.1346/CCMN.2013.0610601.
7. Mckinley IG. Engineering for robustness: an approach to optimising HLW disposal concepts. *Waste Manag*. 1997;17(1):1–8. https://doi.org/10.1016/S0956-053X(97)00026-3.
8. Claret F, Dauzeres A, Jacques D, et al. Modelling of the long-term evolution and performance of engineered barrier system. *EPJ Nucl Sci Technol*. 2022;8:41. https://doi.org/10.1051/epjn/2022038.
9. NDA. Geological Disposal Generic Environmental Safety Case - Main Report.; 2016.
10. International Atomic Energy Agency. *Monitoring of geological repositories for high level radioactive waste*. 2001.
11. White M, Farrow J, Crawford M. *Deliverable D2.1: repository monitoring strategies and screening methodologies*. 2017.
12. Alonso EE, Springman SM, Ng CWW. Monitoring large-scale tests for nuclear waste disposal. *Geotech Geol Eng*. 2008;26(6):817–826. https://doi.org/10.1007/s10706-008-9195-2.
13. Matray JM, Bohner E, Raunio K, et al. *Methodology for qualifying monitoring components. Modem2020 2nd International Conférence about Monitoring in Geological Disposai of Radioactive Waste*. 2019.
14. Cappelli M, Surrenti V. Noncontact Displacement Measurement of Nuclear Waste Canisters in a Geological Disposal by Using an Electromagnetic-Wave Approach. *ASME J Nucl Rad Sci*. 2020;6(4), 041104. https://doi.org/10.1115/1.4047719.
15. Lopes B de CFL, Sachet C, Sentenac P, et al. Preliminary non-intrusive geophysical electrical resistivity tomography surveys of a mock-up scale monitoring of an engineered barrier system at URL Tournemire (Special Publications) *Geol Soc - Mult Roles Clays Radioact Waste Confin*. 2018;482. https://doi.org/10.1144/SP482.11.
16. Lopes B. de C.F.L. , Tarantino A. Design tool for ERT monitoring of bentonite buffer in geological repositories: validation via mock-up scale test. Geomech Energy Environ.
17. Mojid MA, Wyseure GCL, Rose DA. Electrical conductivity problems associated with time-domain reflectometry (TDR) measurement in geotechnical engineering. *Geotech Geol Eng*. 2003;21:243–258. https://doi.org/10.1023/A:1024910309208.
18. Kupfer K, Trinks E, Wagner N, Hübner C. TDR measurements and simulations in high lossy bentonite materials. *Meas Sci Technol*. 2007;18(4):1118–1136. https://doi.org/10.1088/0957-0233/18/4/021.
19. Topp GC, Davis JL, Annan AP. Eletromagnetic determination of soil water content: Measurements in coaxial transmission lines. *Water Resourses Res*. 1980;16:574–582.
20. Ledieu J, De Ridder P, De Clerck P, Dautrebande S. A method of measuring soil moisture by time-domain reflectometry. *J Hydrol*. 1986;88(3-4):319–328.

21. Pozzato A, Tarantino A, McCartney J, Zornberg J. Use of the TDR to evaluate the effect of dry density on the relationship between water content and soil apparent dielectric permittivity. In: *1st European Conference on. Unsatur Soils*. 2008:173–178.
22. Nachum S, Talesnick M, Furman A. Application of TDR in compacted clay soils: issues of dry density, water content range, and calibration. *Can Geotech J*. 2023;60 (3):321–333. https://doi.org/10.1139/cgj-2021-0428.
23. Dirksen C, Dasberg S. Improved calibration of time domain reflectometry soil water content measurements. *Soil Sci Soc Am J*. 1993;57(3):660–667. https://doi.org/10.2136/sssaj1993.03615995005700030005x.
24. Mojid MA, Toride N. Electrical conductivity and dielectric constant of bentonite measured with time-domain reflectometry. *Lowl Technol Int.* 2001;3(2):31–42.
25. Schanz T, Baille W, Tuan LN. Effects of Temperature on Measurements of Soil Water Content with Time Domain Reflectometry. *Geotech Test J*. 2011;34(1):1–8. https://doi.org/10.1520/GTJ103152.
26. Ren GL, Huang WH, Lin ZH, Chung CC. Laboratory assessment of real-time water infiltration measurement in SPV200 bentonite using TDR for high-level radioactive waste disposal design. *Measurement*. 2025;242, 116077. https://doi.org/10.1016/j.measurement.2024.116077.
27. Dobson MC, Ulaby FT, Hallikainen MT, El-Rayes MA. Microwave Dielectric Behavior of Wet Soil-Part II: Dielectric Mixing Models. *IEEE Trans Geosci Remote Sens*. 1985; GE-23(1):35–46. https://doi.org/10.1109/TGRS.1985.289498.
28. Heimovaara TJ, Bouten W, Verstraten JM. Frequency domain analysis of time domain reflectometry waveforms: 2. A four-component complex dielectric mixing model for soils. *Water Resour Res*. 1994;30(2):201–209. https://doi.org/10.1029/93WR02949.
29. Knight JH, Ferré PA, Rudolph DL, Kachanoski RG. A numerical analysis of the effects of coatings and gaps upon relative dielectric permittivity measurement with time domain reflectometry. *Water Resour Res*. 1997;33(6):1455–1460. https://doi.org/10.1029/97WR00435.
30. Mojid MA, Wyseure GCL, Rose DA. The use of insulated time-domain reflectometry sensors to measure water content in highly saline soils. *Irrig Sci*. 1998;18(2):55–61. https://doi.org/10.1007/s002710050044.
31. Nichol C, Beckie R, Smith L. Evaluation of Uncoated and Coated Time Domain Reflectometry Probes for High Electrical Conductivity Systems. *Soil Sci Soc Am J*. 2002;66(5):1454–1465. https://doi.org/10.2136/sssaj2002.1454.
32. García-Siñeriz JL, Mazón MR, Kober F, Sakaki T. Performance of THM monitoring instrumentation in FEBEX bentonite barrier after 18 years of operation under repository-like conditions. *Geomech Energy Environ*. 2019;17:75–89. https://doi.org/10.1016/j.gete.2018.09.008.
33. Jones SB, Or D. Frequency domain analysis for extending time domain reflectometry water content measurement in highly saline soils. *Soil Sci Soc Am J*. 2004;68(5): 1568–1577. https://doi.org/10.2136/sssaj2004.1568.
34. Delage P, Cui YJ, Tang AM. Clays in radioactive waste disposal. *J Rock Mech Geotech Eng*. 2010;2(2):111–123. https://doi.org/10.3724/SP.J.1235.2010.00111.
35. Sun H, Mašín D, Najser J, Nedela V, Navrátilová E. Bentonite microstructure and saturation evolution in wetting-drying cycles evaluated using ESEM, MIP and WRC measurements. *Geotechnique*. 2019;69(8):713–726. https://doi.org/10.1680/jgeot.17.P.253.
36. Nachum S. Soil water potential in geosciences: an overview. *Geosciences*. 2025;15: 123. https://doi.org/10.3390/geosciences15040123.
37. Bulut R, Leong EC. Indirect measurement of suction. *Geotech Geol Eng*. 2008;26: 633–644. https://doi.org/10.1007/s10706-008-9197-0.
38. Yang W, Lunn R, Tarantino A. MEMS sensor-based monitoring system for engineered geological disposal facilities. *Mineral Mag*. 2015;79(6):1475–1483. https://doi.org/10.1180/minmag.2015.079.6.22.
39. Yang W, Lunn RJ, Tarantino A, El Mountassir G. Laboratory testing of a MEMS sensor system for in-situ monitoring of the engineered barrier in a geological disposal facility. *Geosciences*. 2017;7(38):2–9. https://doi.org/10.3390/geosciences7020038.
40. Cardoso R, Sarapajevaite G, Korsun O, Cardoso S, Ilharco L. Sol-gel relative humidity sensors: impact of electrode geometry on performance in soil suction measurements. *J Sens Technol*. 2017;7:1–23. https://doi.org/10.4236/jst.2017.71001.
41. J.M. R. *An introduction to applied and environmental geophysics*. Wiley; 1997.
42. Seladji S, Cosenza P, Tabbagh A, Ranger J, Richard G. The effect of compaction on soil electrical resistivity: a laboratory investigation. *Eur J Soil Sci*. 2010;61(6): 1043–1055. https://doi.org/10.1111/j.1365-2389.2010.01309.x.
43. Parr K, Kulesza SE, Bernhardt-Barry ML. Modified Complex Electrical Resistivity Technique: Applications to Saturated and Unsaturated Soils. *Geotech Test J*. 2024;47 (6). https://doi.org/10.1520/GTJ20230491.
44. Collett LS, Katsube TJ. Electrical parameters of rocks in developing geophysical techniques. *Geophysics*. 1973;38(1):76–91. https://doi.org/10.1190/1.1440336.
45. Archie GE. The electrical resistivity log as an aid in determining some reservoir characteristics. *Trans Am Inst Min Met Eng*. 1942;146:54–61.
46. Chen H, Chou C, Peruzzo L, et al. Development of an ERT - based framework for bentonite buffers monitoring from laboratory tests: 1. Characterizing thermal – hydrological – mechanical processes. *J Geophys Res Solid Earth*. 2025;130(8). https://doi.org/10.1029/2024JB030798.
47. Chen H, Chou C, Peruzzo L, et al. Development of an ERT - based framework for bentonite buffers monitoring from laboratory tests: 2. Quantitative moisture dynamics estimation model. *J Geophys Res Solid Earth*. 2025;30(8):1–21. https://doi.org/10.1029/2024JB030799.
48. Tarantino A, Ridley AM, Toll DG. Field measurement of suction, water content, and water permeability. *Geotech Geol Eng*. 2008;26:751–782. https://doi.org/10.1007/s10706-008-9205-4.
49. Malicki MA, Plagge R, Roth CH. Improving the calibration of dielectric TDR soil moisture determination taking into account the soild soil. *Eur J Soil Sci*. 1996;47: 357–366.
50. Chung CC, Lin CP. Apparent Dielectric Constant and Effective Frequency of TDR Measurements: Influencing Factors and Comparison. *Vadose Zo J*. 2009;8:548–556. https://doi.org/10.2136/vzj2008.0089.
51. Strickland JA. Time-domain reflectometry measurements. *Publ Online*. 1970:11–13.
52. Rhoades JD, Manteghi NA, Shouse PJ, Alves WJ. Estimating soil salinity from saturated soil-paste electrical conductivity. *Soil Sci Soc Am J*. 1989;53:428–433. https://doi.org/10.2136/sssaj1989.03615995005300020019x.
53. Friedman SP. A saturation degree-dependent composite spheres model for describing the effective dielectric constant of unsaturated porous media. *Water Resour Res*. 1998;34(11):2949–2961.
54. Hasted JB. *Aqueous dielectrics*. *Studies in Chemical Physics*. Chapman and Hall; 1973. https://doi.org/10.1002/jobm.19760160714, 16.
55. Giao PH, Chung SG, Kim DY, Tanaka H. Electric imaging and laboratory resistivity testing for geotechnical investigation of Pusan clay deposits. *J Appl Geophys*. 2003; 52(4):157–175. https://doi.org/10.1016/S0926-9851(03)00002-8.
56. Rothfuchs T, Miehe R, Moog H, Wieczorek K. *Geoelectr Investig Bentonite Barrier Satur*. 2004.
57. Cosenza P, Ghorbani A, Florsch N, Revil A. Effects of drying on the low-frequency electrical properties of Tournemire argillites. *Pure Appl Geophys*. 2007;164(10): 2043–2066. https://doi.org/10.1007/s00024-007-0253-0.
58. Fredlund DG, Rahardjo H, Fredlund MD. *Unsaturated soil mechanics in engineering practice*. John Wiley & Sons; 2012.
59. Guo JY, Shi B, Sun MY, et al. Soil total suction sensing using fiber-optic technology. *Geoderma*. 2023;439, 116687. https://doi.org/10.1016/j.geoderma.2023.116687.
60. Winston PW, Bates DH. Saturated Solutions For the Control of Humidity in Biological Research. *Ecology*. 1960;41(1):232–237.
61. Greenspan L. Humidity fixed points of binary saturated aqueous solutions. *J Res Natl Bur Stand Sect A Phys Chem*. 1977;81A(1):89–96. https://doi.org/10.6028/jres.081A.011.
62. Garitte B, Weber H, Müller HR. *Requir Manuf QC Buffer Compon Report LUCOEX WP2*. 2015.
63. Wang Q, Tang AM, Cui YJ, Delage P, Gatmiri B. Experimental study on the swelling behaviour of bentonite/claystone mixture. *Eng Geol*. 2012;124(1):59–66. https://doi.org/10.1016/j.enggeo.2011.10.003.
64. Zegelin SJ, White I, Jenkins DR. Improved field probes for soil water content and electrical conductivity measurement using time domain reflectometry. *Water Resour Res*. 1989;25(11):2367–2376.
65. Gallipoli D, Wheeler SJ, Karstunen M. Modelling the variation of degree of saturation in a deformable unsaturated soil. *Geotechnique*. 2003;53(1):105–112. https://doi.org/10.1680/geot.2003.53.1.105.
66. van Genuchten M. A closed-form equation for predicting the hydraulic conductivity of unsaturated soils. *Soil Sci Soc Am J*. 1980;44:892–898. https://doi.org/10.2136/sssaj1980.03615995004400050002x.
67. Ko H, Choo H, Ji K. Effect of temperature on electrical conductivity of soils – role of surface conduction. *Eng Geol*. 2023;321(May), 107147. https://doi.org/10.1016/j.enggeo.2023.107147.
68. Campbell RB, Bower CA, Richards LA. Change of electrical conductivity with temperature and the relation of osmotic pressure to electrical conductivity and ion concentration for soil extracts. *Soil Sci Soc Am Proc*. 1948;13:66–69.
69. Corwin DL, Lesch SM. Apparent soil electrical conductivity measurements in agriculture. *Comput Electron Agric*. 2005;46:11–43. https://doi.org/10.1016/j.compag.2004.10.005.
70. Hayley K, Bentley LR, Gharibi M, Nightingale M. Low temperature dependence of electrical resistivity: Implications for near surface geophysical monitoring. *Geophys Res Lett*. 2007;34:1–5. https://doi.org/10.1029/2007GL031124.
71. Ma R, McBratney A, Whelan B, Minasny B, Short M. Comparing temperature correction models for soil electrical conductivity measurement. *Precis Agric*. 2011; 12:55–66. https://doi.org/10.1007/s11119-009-9156-7.
72. Persson M, Berndtsson R. Texture and electrical conductivity effects on temperature dependency in time domain reflectometry. *Soil Sci Soc Am J*. 1998;62(4):887–893.
73. Samouëlian A, Cousin I, Tabbagh A, Bruand A, Richard G. Electrical resistivity survey in soil science: A review. *Soil Tillage Res*. 2005;83:173–193. https://doi.org/10.1016/j.still.2004.10.004.
74. Mojid MA, Cho H. Effects of water content and temperature on the surface conductivity of bentonite clay. *Soil Res*. 2012;50(1):44–49. https://doi.org/10.1071/SR11228.
75. Saarenketo T. Electrical properties of water in clay and silty soils. *J Appl Geophys*. 1998;40:73–88. https://doi.org/10.1016/S0926-9851(98)00017-2.
76. Leroy P, Maineult A, Mendieta A, Jougnot D. A mechanistic model for the complex conductivity of clay materials. I. Theory. *Geophys J Int*. 2024;241(1):110–132. https://doi.org/10.1093/gji/ggae428.
77. Glover PWJ, Hole MJ, Pous J. A modified Archie's law for two conducting phases. *Earth Planet Sci Lett*. 2000;180:369–383. https://doi.org/10.1016/S0012-821X(00)00168-0.
78. Van Loon LR, Mibus J. A modified version of Archie's law to estimate effective diffusion coefficients of radionuclides in argillaceous rocks and its application in safety analysis studies. *Appl Geochem*. 2015;59:85–94. https://doi.org/10.1016/j.apgeochem.2015.04.002.
79. Van Loon LR, Mibus J. A modified version of Archie's law to estimate effective diffusion coefficients of radionuclides in argillaceous rocks and its application in safety analysis studies. *Appl Geochem*. 2015;59:85–94. https://doi.org/10.1016/j.apgeochem.2015.04.002.